He, J.; Zhang, M.; Primo Arnau, AM.; García Gómez, H.; Li, Z. (2018). Selective photocatalytic benzene hydroxylation to phenol using surface- modified Cu2O supported on graphene. Journal of Materials Chemistry A. 6(40):19782-19787. https://doi.org/10.1039/c8ta07095d

Selective Photocatalytic Benzene Hydroxylation to Phenol Using Surface-Modified Cu_2O Supported on Graphene

Jinbao He,[a] Min Zhang,[b] Ana Primo,[a] Hermenegildo García, *[a] Zhaohui Li *[b]

[a] Instituto de Tecnología Química, Consejo Superior de Investigaciones Científicas-Universitat Politecnica de Valencia, Av. De los Naranjos s/n, 46022 Valencia, Spain

[b] Research Institute of Photocatalysis, State Key Laboratory of Photocatalysis on Energy and Environment, College of Chemistry, Fuzhou University, Fuzhou, 350116, P. R. China.

Abstract

The photocatalytic activity for benzene hydroxylation to phenol by hydrogen peroxide has been evaluated using a series of photocatalysts based on defective graphene. The series includes defective graphene containing or not Au and Cu_2O nanoparticles. The later exhibits the highest activity, but a very low phenol yield as consequence of the occurrence of a large degree of mineralization. A considerably increase in phenol selectivity was achieved by modifying the surface of the Cu_2O nanoparticles supported on defective graphene with long-chain alkanethiols. Under the optimal conditions using an octanethiol-modified Cu_2O-graphene photocatalyst, a selectivity to phenol about 64 % at 30 % benzene conversion was achieved. This remarkable selectivity was proposed to derive from the larger hydrophobicity of the alkanethiol-modified Cu_2O-graphene

photocatalyst that favors the preferential benzene adsorption versus adsorption of phenol and hydroxybenzenes.

Introduction

Graphenes have an increasing importance in photocatalysis, either as additive in small percentage to increase the efficiency of semiconductors or as photoactive component in the system.[1, 2] While ideal graphene is a zero-band semiconductor, the presence of defects and dopant elements can introduce a semiconducting behavior.[3-6] The photocatalytic activity of graphene oxide has been widely studied, but it has been reported that doped, defective graphenes can exhibit also a notable photocatalytic activity.[7-12]

In this context, it has been shown that pyrolysis of natural polysaccharides, some of them residues from the fishery industry or biomass wastes, converts them into turbostratic graphitic carbons that upon sonication afford high yields of defective graphenes.[13-15] Depending on the polysaccharide, this precursor can act simultaneously as source of C and a dopant element, such as N and S in the case of chitosan and carrageen, respectively.[16-18] It has been found that N- or P-doped graphenes obtained through this pyrolysis procedure can generate hydrogen from aqueous solutions of sacrificial electron donors.[19-21]

In addition, these defective graphenes containing in a few percent Au or Cu_2O nanoparticles strongly grafted have a remarkable photocatalytic activity for the overall water splitting and the photo-assisted methanation of CO_2.[22, 23] Available evidence

supports that the mechanism of the photocatalytic reaction occurs through photoinduced charge separation with the generation of electrons in the conduction band and positive holes in the valence band.

In view of the photoactivity of these defective graphenes, it would be of interest to explore further the performance of these materials for other photocatalytic reactions. In this regard, it has been reported that defective graphenes can promote the photo-assisted Fenton-like degradation of phenol by solar light.[24] The available data indicates that the reaction involves the generation of hydroxyl radicals that attack to phenol forming hydroquinone and p-benzoquinone. Continuing with this research it would be important to determine if this ability of defective graphenes to generate hydroxyl radicals from hydrogen peroxide and the possibility that these materials offer to tune their surface properties can be exploited to promote photocatalytic hydroxylation of benzene to form phenol. Phenol is industrially obtained in two steps from benzene through the intermediacy of cumene.[25] The development of a one-step, selective oxidation of benzene to phenol will be of large importance, especially when such a reaction can be driven by solar energy.[26-37]

In the present manuscript the preparation and photocatalytic activity for benzene hydroxylation using H_2O_2 over a series of graphenes supporting metals in which the surface has been modified will be presented. It will be shown that by appropriate tuning of the surface hydrophilicity/hydrophobicity, graphene-based photocatalysts having a notable selectivity to phenol at medium conversions can be obtained.

Results and Discussion

The list of samples prepared, their analytical data and some relevant properties are summarized in Table 1. These samples were prepared from alginate that was submitted to pyrolysis under inert atmosphere, either in the absence of metals, or containing adsorbed various amounts of $AuCl_4^-$ and Cu^{2+} salts. As commented in the introduction, it has been reported that pyrolysis of alginate and subsequent sonication of the graphitic carbon residue affords defective graphenes. The present characterization data coincide with those reported in the literature.[38, 39] The relatively low C content is due to the presence of adsorbed H_2O onto the ambient equilibrated graphene samples. It has also been found by XPS that the samples of this defective graphene (*d*G) contain in its composition about 10 % of residual oxygen covalently attached to the graphene carbons. Analysis of C1s peak in XPS shows the presence of graphitic C as predominant component in about 70 %, accompanied by other components corresponding to C atoms bonded to O, either with single or multiple bonds. The presence of defects is reflected in the Raman spectra of *d*G by the observation of the D peak at about 1350 cm^{-1} accompanying the characteristic 2D and G bands at 2700 and 1590 cm^{-1}, respectively. The density of defects can be quantitatively measured by the relative intensity of the G vs. the D band that in the present case is 1.18. This I_G/I_D ratio is in the order of the values previously reported for other defective graphenes and somewhat higher (lesser defect density) than those typical for reduced graphene oxide (rGO) reported in the literature that are about 0.9. The typical 2D morphology of *d*G was observed by transmission electron microscopy, where sheets of single and few-layers graphene with micrometric lateral size were observed.

Table 1. Analytical data and some relevant properties of the samples prepared in the present study.

Sample	Metal[a] (wt%)	N (wt%)	C (wt%)	S (wt%)	Average particle size[b] (nm)	Alkanethiol [c](at%)	Heating absorption (J/g)
*d*G	0	0.24	68.69	0.68			
Au/*d*G	0.53				7.2		
Cu_2O/*d*G	6.6	0.21	60.16	0.61	11.4		32.70
Cu_2O-8/*d*G	6.6	0.49	76.88	0.91		6.77	24.80
Cu_2O-12/*d*G	6.6	0.23	56.57	0.87		5.76	24.17
Cu_2O-16/*d*G	6.6	0.21	56.55	0.86		5.45	22.59

[a] Calculated from ICP analysis; [b] calculated from TEM images; [c] calculated from combustion elemental analysis. Molecules of alkanethiol per 100 Cu atoms.

Au/*d*G and Cu_2O/*d*G were prepared by depositing on preformed *d*G samples, Au and Cu nanoparticles (NPs) obtained by chemical reduction of $AuCl_4^-$ and Cu^{2+} salts following the so-called polyol method using ethylene glycol as reducing agent at 120 ^oC for 24 h. It has been shown that the polyol reduction is a convenient and reliable method to obtain metal NPs.[40-43] In the presence of *d*G, these metal NPs become supported on this defective graphene. The metal content in the samples was determined by ICP analysis after dissolving the metal with *aqua regia*. In the case of Au, three different Au/*d*G differing in the Au content were prepared.

For the samples at the highest metal loadings, the presence of metal on the defective graphene samples can be demonstrated by XRD. In the case of Au/*d*G at the highest metal loading, the presence of Au was determined by recording in XRD the peaks corresponding to the expected cubic phase of this noble metal. In contrast to the case of

Au/*d*G, XRD of Cu samples immediately after preparation showed besides the peaks corresponding to Cu(0) others indicating the presence of Cu_2O. Figure 1 shows the XRD patterns of Au/*d*G and Cu_2O/*d*G. This oxide could derive either from the incomplete reduction of Cu^{2+} ions in the polyol method or from the oxidation of the outermost layers Cu NPs upon exposure of the sample to the ambient. Due to the presence of cuprous oxide that is a well-known visible-light semiconductor, these samples containing Cu were denoted as Cu_2O/*d*G.

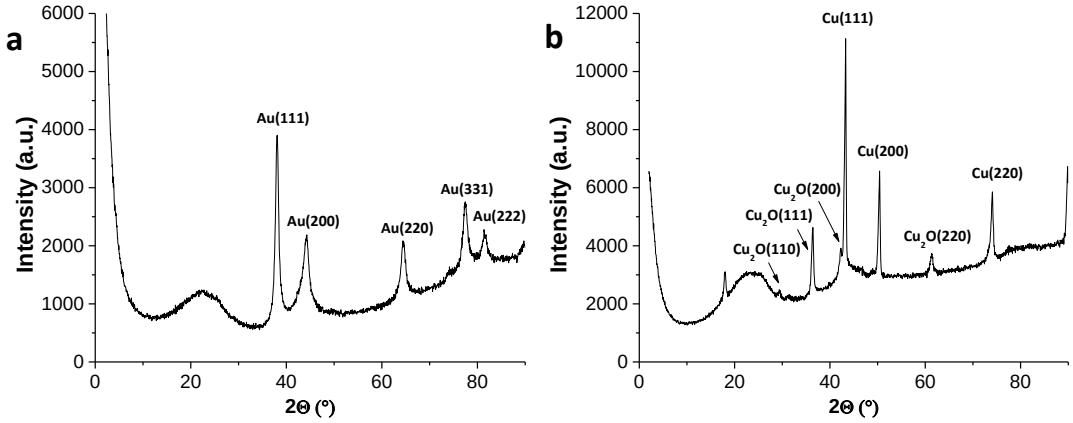

Figure 1. XRD patterns of Au/*d*G (a) and Cu_2O/*d*G (b).

The list of samples under study was completed with three surfactant modified Cu_2O/*d*G photocatalysts that were prepared by sonication of freshly prepared Cu_2O/*d*G samples in ethanol solutions of long chain alkyl thiols from 8 to 16 carbon atoms in a Cu-to-S atomic ratio of 1. Based on the existing precedents, it was expected that thiol molecules will bind to the Cu_2O NPs due to the strong Cu-S interaction. In this way, the polarity of the Cu_2O NP surfaces could be modified, increasing the hydrophobicity of the Cu_2O NPs. The samples are denoted as Cu_2O-x/*d*G, where x indicates the number of carbon atoms of the surfactant.

Anchoring of alkanethiols on Cu_2O-x/*d*G was quantified by determining the increase in the S content compared to the parent Cu_2O/*d*G sample and also by comparison of the thermogravimetric profiles of the Cu_2O-x/*d*G samples with respect to that of Cu_2O/*d*G. The results are summarized in Table 1. As indicated above, the purpose of introducing long alkyl chains is to enhance the hydrophobicity of the Cu_2O-x/*d*G samples respect to the parent Cu_2O/*d*G and, in this way, control the product distribution in the (photo)catalytic benzene hydroxylation. A first experimental evidence supporting this change in the surface polarity of the Cu_2O-x/*d*G materials respect to Cu_2O/*d*G can be inferred from the thermogravimetric profiles shown in Figure 2. As it can be seen there, the parent Cu_2O/*d*G sample exhibits a higher weight loss from 150 to 300 ^oC that can be attributed to a higher water desorption in this Cu_2O/*d*G sample respect to Cu_2O-x/*d*G materials. At higher temperatures, the weight loss of Cu_2O-x/*d*G is higher than that of Cu_2O/*d*G due to the combustion decomposition of the alkyl chain of thiol. In this way, the weight loss from 300 till 700 ^oC can be also used to quantify the weight percentage of alkanethiol present in the samples. This estimation coincides reasonably well with that based on the increment in the S content determined by combustion chemical analysis. These estimations indicate that there is about 5-7 molecules of alkanethiol per 100 Cu atoms in the Cu_2O-x/*d*G samples (see Table 1).

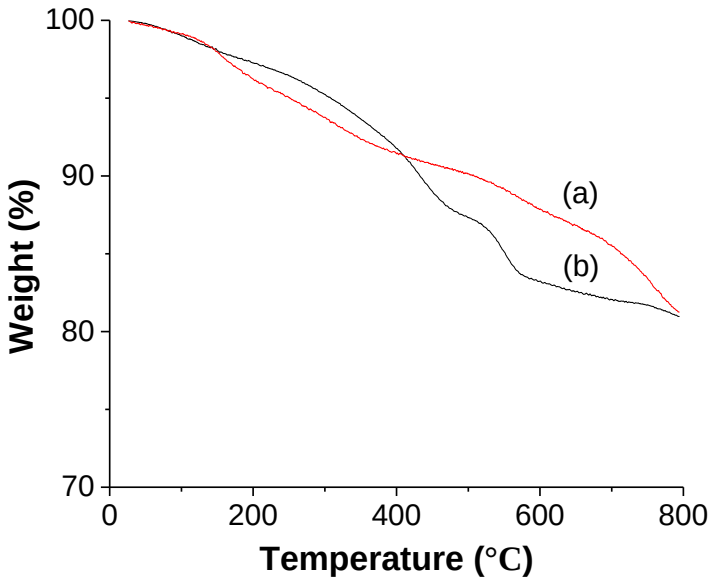

Figure 2. TG results of Cu_2O/*d*G (a) and Cu_2O-8/*d*G(b) obtained under N_2 atmosphere.

Further evidence of the influence of the presence alkanethiols and the chain length in the increase in the surface hydrophobicity was obtained by measuring the heat of water adsorption at low H_2O coverages (Table 1). It was measured that this heat of adsorption at low coverages decreases, initially abruptly upon thiolation from a value of 32.70 to 24.80 $J \times g^{-1}$ going from the parent Cu_2O/*d*G to Cu_2O-8/*d*G and, then, more gradually from to 24.80 to 22.59 $J \times g^{-1}$ from Cu_2O-8/*d*G to Cu_2O-16/*d*G. These values are in good agreement with the polarity changes that could be predicted based on the configuration of the Cu_2O-x/*d*G surface.

The presence of Au or Cu_2O NPs on the surface of *d*G, their distribution and their particle size was determined by transmission electron microscopy of the Au/*d*G and Cu_2O/*d*G samples. Figure 3 shows selected images at different magnifications to illustrate the textural characteristic of the samples. As it can be seen there, in the case of Au, smaller NPs of 7.2 nm average size well distributed on single sheets *d*G can be observed.

In contrast, in the case of Cu_2O, much larger particles and a broad size distribution was observed. This difference in the behavior of Au and Cu is also in accordance with the literature and the expected behavior of salts of these two metals in the polyol reduction method.

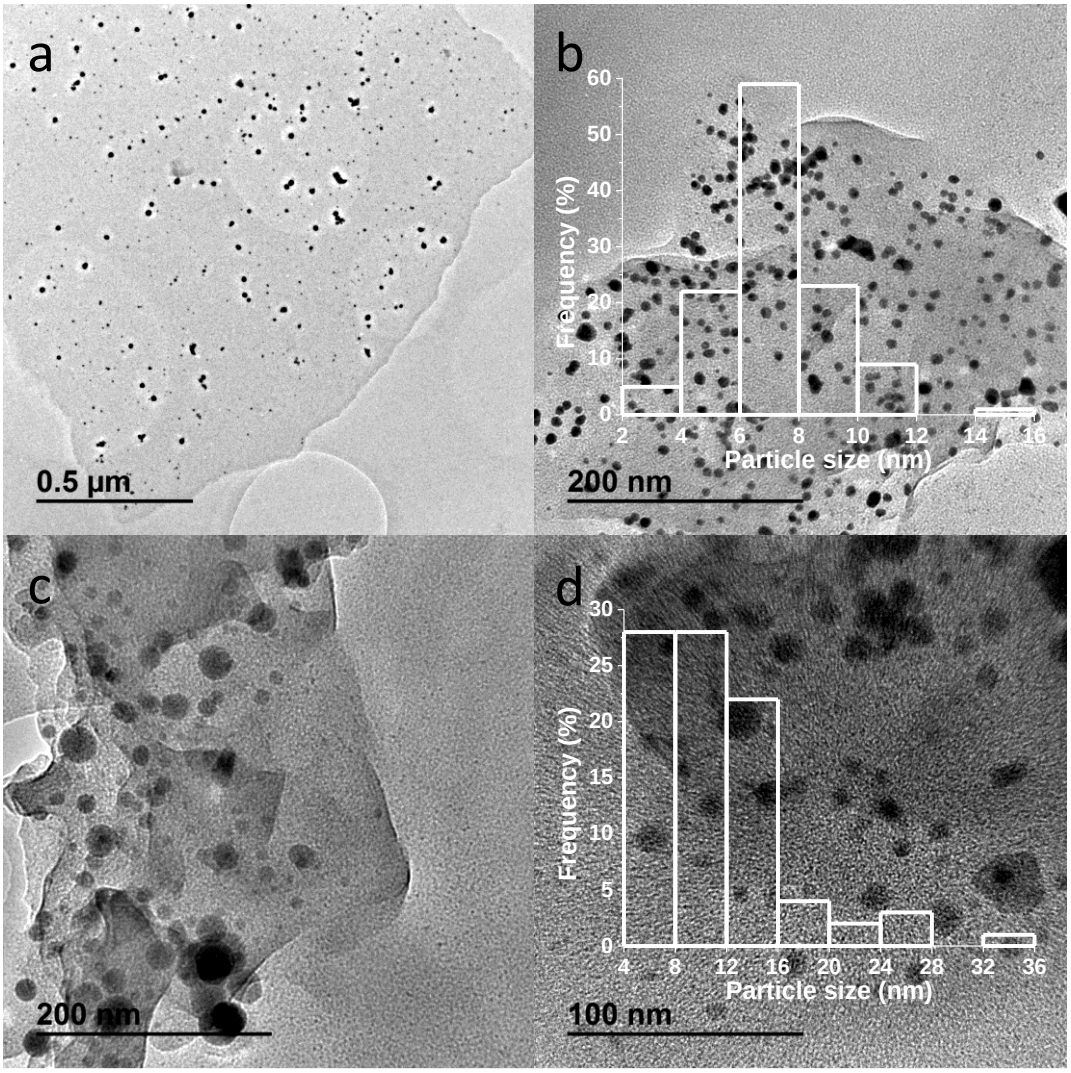

Figure 3. TEM images of Au/*d*G sample (a,b) and Cu_2O/*d*G (c,d) at different magnifications. The insets show the statistical particle size distributions of the two samples respectively.

Photocatalytic activity

The set of samples prepared was evaluated with respect to their (photo)catalytic activity to oxidize benzene by hydrogen peroxide. The results are provided in Tables 2 and 3, depending on whether the reactions were carried out upon visible light irradiation using a LED or in the dark in the case of the surfactant-modified Cu_2O-x/*d*G samples. As it can be seen there, although even *d*G exhibits photocatalytic activity, this activity increases substantially by the presence of metals either Au or Cu_2O. The increase of benzene conversion was particularly high in the case of Cu_2O/*d*G. However, in spite of the moderate to high benzene conversion, the yield to phenol was always very low (about 1 %) due to overoxidation of phenol to complete mineralization to CO_2. As can be seen in Table 2, most of the conversion of benzene with these photocatalysts corresponds to unwanted mineralization that accounts for almost the whole benzene conversion.

In an attempt to gain control on the selectivity of the process and to direct the process towards the wanted phenol production, the most active photocatalyst, Cu_2O/*d*G, was functionalized with alkanethiols of increasing chain length in the range from 8 to 16 carbons. It was reasoned that an increase in the hydrophobicity of the surface of the photocatalyst should favor preferential adsorption of low polarity substrates, like benzene, over the more polar ones, like hydroxyl and polyhydroxy benzene. Desorption of phenol away from the photocatalyst surface should increase its selectivity. In this way, after formation of phenol, this compound could be desorbed from the photocatalyst surface by competition with benzene. This surface modification was performed by using long chain thiols, based on the well-known affinity of Cu^+ and other soft metal ions for sulfur ligands.

As it could be anticipated, modification of Cu_2O/*d*G by alkanethiols decreased the photocatalytic activity due to the masking of some active centers. However, the photocatalytic activity of these Cu_2O-x/*d*G samples was still notable and, importantly, it even increased with the length of the alkyl chain. For Cu_2O-12/*d*G and Cu_2O-16/*d*G the photocatalytic activity was similar or even higher than that of Cu_2O/*d*G, a fact that could be attributed for the more favorable adsorption of benzene on these materials that would compensate the effect of Cu_2O surface coverage.

However, the most remarkable effect of the presence of alkanethiols is the over one-order of magnitude increase in the phenol yield that is a consequence of the phenol selectivity. In the case of Cu_2O-8/*d*G at moderate conversions, phenol selectivity values well over 50 % were achieved. The percentage of benzene mineralization was concomitantly decreased, reaching values as low as about 10 % at over 30 % benzene conversion. This behavior can be rationalized in general terms as derived from the control of the surface hydrophilicity/hydrophobicity and the different polarity of substrates and primary products. As far as we know these phenol selectivity values are without precedent and illustrate the potential that graphene-based photocatalysts offer for the selective production of high-added value chemicals by controlling surface polarity.

The effect of light on the process is clearly demonstrated by comparing the results of the photocatalytic benzene hydroxylation with those in the dark. Although the reaction takes place in significant degree also in the dark, benzene conversions are somewhat lower in the case of the non-irradiated reactions. Moreover, phenol selectivity are notably much lower in the dark respect the irradiated reactions accompanied by a larger mineralization degree. Thus, the photocatalytic reaction gives significantly better results.

The difference between the dark and the photocatalytic reaction shows the difference in the rate determining steps and activation barriers between the two processes. It seems that in the case of the dark reaction the reaction rates for benzene or phenol reaction are not as different as in the case of the photocatalytic reaction.

The cycling test over Cu_2O-8/*dG* showed that there was no obvious change of benzene conversion as well as the yield to phenol after three successive runs (Figure 4).

Table 2. The catalytic results obtained under the LED illumination.

Catalyst	Time (h)	Benzene conv.(%)	Phenol yield(%)	Phenol selec.(%)	Benzoquinone yield (%)	Mineralization (%)[a]
*d*G	16	10.74	0.40	3.72	0.00	10.30
Au/*d*G	16	30.06	0.46	1.53	0.00	29.60
Cu_2O/*d*G	16	61.28	1.22	1.99	0.16	59.90
Cu_2O-8/*d*G	16	30.18	19.30	63.94	0.47	10.40
Cu_2O-12/*d*G	16	55.13	10.63	19.27	0.15	44.35
Cu_2O-16/*d*G	16	70.64	14.82	20.98	2.10	53.71

[a]Mineralization (%) = (initial amount of benzene – residual benzene – phenol – benzoquinone) / (initial amount of benzene) × 100 %

Table 3. The catalytic results obtained in the dark.

Catalyst	Time (h)	Benzene conv.(%)	Phenol yield(%)	Phenol selec.(%)	Benzoquinone yield (%)	Mineralization (%)[a]
*d*G	16	10.72	2.09	19.53	0.01	10.89
Au/*d*G	16	41.40	3.08	7.45	0.03	39.81
Cu_2O/*d*G	16	43.79	6.43	14.69	7.86	31.04
Cu_2O-8/*d*G	16	27.85	6.31	22.65	19.24	2.30
Cu_2O-12/*d*G	16	50.00	7.52	15.04	0.01	42.46
Cu_2O-16/*d*G	16	58.41	5.79	9.91	0.05	52.58

[a]Mineralization (%) = (initial amount of benzene – residual benzene – phenol – benzoquinone) / (initial amount of benzene) × 100 %

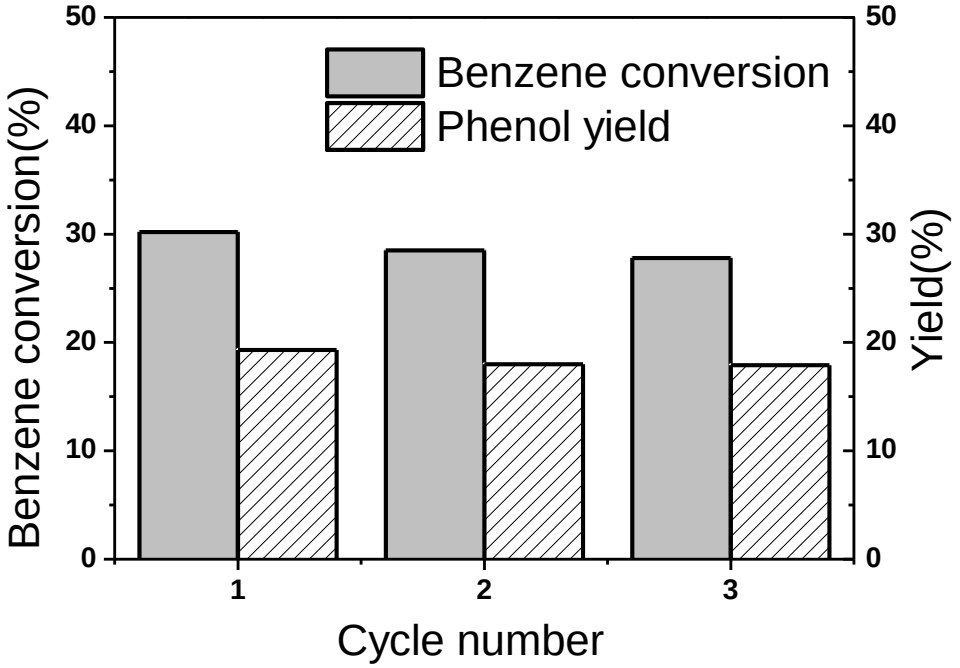

Figure 4. Cycling test on Cu_2O-8/*d*G for Benzene Hydroxylation.

Conclusions

The present manuscript constitutes an additional example showing the increase in the photocatalytic efficiency of semiconductors by the presence of graphenes as consequence of the increase in the efficiency of the charge separation and the decrease of charge recombination. In the present case, this effect of graphene has been applied to carry out photocatalytic hydroxylation of benzene to phenol. It has been found that the much higher reactivity of phenol results in very low phenol yields and selectivity values and the occurrence of a large degree of mineralization. However, modification of the surface polarity by attachment of long alkyl chains can serve to control the hydrophilicity/hydrophobicity of the reaction centers and as favor the adsorption of the substrates versus that of the product. In this way, phenol selectivity as high as 63.94 % at about 30 % benzene conversion could be achieved. Although the benzene hydroxylation also occurs in the dark promoted by the photocatalyst, the selectivity to phenol is about

four times lower and mineralization prevails. Thus, it is the combination of light and surface modification what is responsible for the notable selectivity on phenol in the reaction of benzene.

Experimental section

Synthesis of *d*G

Alginic acid sodium salt from brown algae (Sigma) was pyrolysed under Ar atmosphere using the following program: annealing at 200 ^{o}C for 2 h and then heating with a rate of 10 ^{o}C min^{-1} up to 900 ^{o}C for 2 h. The sample was allowed to cool at room temperature under inert atmosphere.

Synthesis of Au/*d*G

*d*G from alginate pyrolysis (100 mg) was added to ethylene glycol (40 mL) and the mixture was sonicated at 700 W for 1 h to obtain dispersed *d*G. $HAuCl_4$ (5.93 mg) was added to the reaction mixture and Au metal reduction was then performed at 120 ^{o}C for 24 h with continuous stirring. The Au/*d*G samples were finally separated by filtration and washed exhaustively with water and acetone. The resulting material was dried in a vacuum desiccator overnight to remove the remaining water.

Synthesis of Cu_2O/*d*G

*d*G from alginate pyrolysis (100 mg) was added to ethylene glycol (40 mL) and the mixture was sonicated at 700 W for 1 h to obtain dispersed *d*G. $Cu(NO_3)_2{\cdot}H_2O$ (42.0 mg) was added to the reaction mixture and Cu metal reduction was then performed at 120 ^{o}C for 24 h with continuous stirring. The Au/*d*G samples were finally separated by filtration and

washed exhaustively with water and acetone. The resulting material was dried in a vacuum desiccator overnight to remove the remaining water.

Synthesis of Cu_2O-x/*d*G

Cu_2O/*d*G (100 mg) was sonicated in 200 ml ethanol solution for 1.5 h to obtain dispersed sample. Then a certain amount of alkanethiol with a mole rate of 1:1 for Cu atom and thiol, (17.9 µL 1-octanethiol, 23.9 µL 1-dodecanethiol, 30.8 µL 1-hexadecanethiol, respectively), was added into the solution and the mixture was sonicated for another 1.5 h. After that, the samples were separated by filtration and washed exhaustively with water and acetone. The resulting material was dried in a vacuum desiccator overnight to remove the remaining water.

Characterization techniques

TEM images were recorded by using a Philips CM 300 FEG system with an operating voltage of 100 kV. X-ray diffraction (XRD) patterns were obtained by using a Philips X' Pert diffractometer and copper radiation (CuK_a=1.541178 A°). Quantitative ICP-OES measurements were performed by using a 715-ES Varian apparatus. Combustioin elemental analysis was carried out with Euro EA3000 Elemental Analyzer (EuroVector), using sulfanilamide as a reference. TG was performed with a Mettler Toledo TGA/SDTA 851e device in the temperature range from 20 to 800 ^oC at a speed of 10 $^oC\ min^{-1}$ under N_2 atmosphere. Water heating absorption measurement was performed with C80 immersion calorimeter.

Photocatalytic reactions

The photocatalytic reactions were carried out in a PCX50B Discover system. In a typical catalytic process, deionized water (5 mL) and benzene (1 mmol) were transferred to a Schlenk tube containing catalyst (5 mg). After stirring for 30 min, H_2O_2 (30%, 1 mmol) was added. The system was irradiated by a white light LED lamp (130 mW×cm^{-2}) at room temperature (Fig. S1). After reaction, 5 mL of acetonitrile was poured into the reaction system to turn the biphasic system to a single-phase one. After removal of the catalyst, the solution was analyzed by High Performance Liquid Chromatography (Alliance e2695, Waters) equipped with a Photo-Diode Array Detector using a C-18 column. The column temperature was kept at 30 °C. A mixture of acetonitrile and water in a volume ratio of 70:30 was used as the eluent. Benzene, phenol, benzoquinone were detected by the Photo-Diode Array Detector at 213, 215 and 243 nm, respectively. The gaseous product (CO_2) was detected by a GC-TCD (Shimadzu GC-2014) with a TDX-01 packed column. The catalyst was washed with ethanol and then dried under vacuum at 60 °C for 10 h and then reused in the next run.

Acknowledgements

J.H. thanks the Chinese Scholarship Council for a graduate scholarship. Financial support by the Spanish Ministry of Economy and Competitiveness (Severo Ochoa, CTQ2015-69653-CO2-R1 and Grapas) and Generalitat Valenciana (Prometeo 2017-083) is gratefully acknowledged. This work was also supported by NSFC (21872031, U1705251) and 973 Program (2014CB239303) of P. R. China.

References

1. Q. Xiang, J. Yu and M. Jaroniec, *Chem. Soc. Rev.*, 2012, **41**, 782-796.
2. N. Zhang, Y. Zhang and Y. J. Xu, *Nanoscale*, 2012, **4**, 5792-5813.
3. A. Nourbakhsh, M. Cantoro, T. Vosch, G. Pourtois, F. Clemente, M. H. van der Veen, J. Hofkens, M. M. Heyns, S. De Gendt and B. F. Sels, *Nat. Nanotech.*, 2010, **21**, 435203.
4. L. K. Putri, W.-J. Ong, W. S. Chang and S.-P. Chai, *Appl. Surf. Sci.*, 2015, **358**, 2-14.
5. X. Wang, G. Sun, P. Routh, D. H. Kim, W. Huang and P. Chen, *Chem. Soc. Rev.*, 2014, **43**, 7067-7098.
6. T. F. Yeh, C. Y. Teng, S. J. Chen and H. Teng, *Adv. Mater.*, 2014, **26**, 3297-3303.
7. D. Chen, H. Zhang, Y. Liu and J. Li, *Energy Environ. Sci* . 2013, **6**, 1362.
8. A. Iwase, Y. H. Ng, Y. Ishiguro, A. Kudo and R. Amal, *J. Am. Chem. Soc.*, 2011, **133**, 11054-11057.
9. D. Qu, M. Zheng, P. Du, Y. Zhou, L. Zhang, D. Li, H. Tan, Z. Zhao, Z. Xie and Z. Sun, *Nanoscale*, 2013, **5**, 12272-12277.
10. Y. Xu, Y. Mo, J. Tian, P. Wang, H. Yu and J. Yu, *Appl. Catal., B*, 2016, **181**, 810-817.
11. X. Li, J. Yu, S. Wageh, A. A. Al‐Ghamdi and J. Xie, *Small*, 2016, **12**, 6640-6696.
12. Y. T. Liang, B. K. Vijayan, K. A. Gray and M. C. Hersam, *Nano Lett.*, 2011, **11**, 2865-2870.
13. A. Dhakshinamoorthy, A. Primo, P. Concepcion, M. Alvaro and H. Garcia, *Chem. Eur. J.*, 2013, **19**, 7547-7554.
14. A. Primo, P. Atienzar, E. Sanchez, J. M. Delgado and H. Garcia, *Chem. Commun.*, 2012, **48**, 9254-9256.
15. A. Primo, E. Sánchez, J. M. Delgado and H. García, *Carbon*, 2014, **68**, 777-783.
16. A. Dhakshinamoorthy, M. Latorre-Sanchez, A. M. Asiri, A. Primo and H. Garcia, *Catal. Commun.*, 2015, **65**, 10-13.
17. I. Esteve-Adell, B. Crapart, A. Primo, P. Serp and H. Garcia, *Green Chem.*, 2017, **19**, 3061-3068.
18. A. Primo, F. Neatu, M. Florea, V. Parvulescu and H. Garcia, *Nat. Commun.*, 2014, **5**, 5291.
19. A. Garcia, J. Albero and H. García, *ChemPhotoChem*, 2017, **1**, 388-392.
20. C. Lavorato, A. Primo, R. Molinari and H. Garcia, *Chem. Eur. J.*, 2014, **20**, 187-194.
21. M. Latorre-Sanchez, A. Primo and H. Garcia, *Angew. Chem. Int. Ed.*, 2013, **52**, 11813-11816.
22. D. Mateo, I. Esteve-Adell, J. Albero, J. F. Royo, A. Primo and H. Garcia, *Nat. Commun.*, 2016, **7**, 11819.
23. D. Mateo, J. Albero and H. García, *Energy Environ. Sci* . 2017, **10**, 2392-2400.
24. J. C. Espinosa, S. Navalón, M. Álvaro and H. García, *ChemCatChem*, 2016, **8**, 2642-2648.

25. R. J. Schmidt, *Appl. Catal., A*, 2005, **280**, 89-103.
26. L. Balducci, D. Bianchi, R. Bortolo, R. D'Aloisio, M. Ricci, R. Tassinari and R. Ungarelli, *Angew. Chem. Int. Ed.*, 2003, **115**, 5087-5090.
27. B. Liptakova, M. Hronec and Z. Cvengrošová, *Catal. Today*, 2000, **61**, 143-148.
28. S.-i. Niwa, M. Eswaramoorthy, J. Nair, A. Raj, N. Itoh, H. Shoji, T. Namba and F. Mizukami, *Science*, 2002, **295**, 105-107.
29. G. Wen, S. Wu, B. Li, C. Dai and D. S. Su, *Angew. Chem. Int. Ed.*, 2015, **54**, 4105-4109.
30. Z. Kang, E. Wang, B. Mao, Z. Su, L. Gao, L. Niu, H. Shan and L. Xu, *Appl. Catal., A*, 2006, **299**, 212-217.
31. Q. Wei, H. Fan, F. Qin, Q. Ma and W. Shen, *Carbon*, 2018, **133**, 6-13.
32. G. Panov, G. Sheveleva, A. e. a. Kharitonov, V. Romannikov and L. Vostrikova, *Appl. Catal., A*, 1992, **82**, 31-36.
33. J.-H. Yang, G. Sun, Y. Gao, H. Zhao, P. Tang, J. Tan, A.-H. Lu and D. Ma, *Energy Environ. Sci .* 2013, **6**, 793-798.
34. D. S. Su, G. Wen, S. Wu, F. Peng and R. Schlögl, *Angew. Chem. Int. Ed.*, 2017, **56**, 936-964.
35. D. Wang, M. Wang and Z. Li, *ACS Catal.*, 2015, **5**, 6852-6857.
36. Z. Zheng, B. Huang, X. Qin, X. Zhang, Y. Dai and M.-H. Whangbo, *J. Mater. Chem*, 2011, **21**, 9079.
37. X. Chen, J. Zhang, X. Fu, M. Antonietti and X. Wang, *J. Am. Chem. Soc.*, 2009, **131**, 11658-11659.
38. S. Frindy, A. El Kadib, M. Lahcini, A. Primo and H. García, *Catal. Sci. Technol.*, 2016, **6**, 4306-4317.
39. A. Primo, I. Esteve‐Adell, S. N. Coman, N. Candu, V. I. Parvulescu and H. Garcia, *Angew. Chem. Int. Ed.*, 2016, **128**, 617-622.
40. S. Frindy , A. El Kadib, M. Lahcini, A. Primo and H. García, *ChemistrySelect*, 2016, **1**, 157-162.
41. J. F. Blandez, I. Esteve-Adell, M. Alvaro and H. García, *Catal. Sci. Technol.*, 2015, **5**, 2167-2173.
42. P. Divya and S. Ramaprabhu, *J. Mater. Chem. A*, 2014, **2**, 4912-4918.
43. Y.-Y. Shen, Y. Sun, L.-N. Zhou, Y.-J. Li and E. S. Yeung, *J. Mater. Chem. A*, 2014, **2**, 2977-2984.